Available online at www.sciencedirect.com
ScienceDirect
Icarus 195 (2008) 792–801
ICARUS
www.elsevier.com/locate/icarus

Laboratory studies of methane and ethane adsorption and nucleation onto organic particles: Application to Titan's clouds

Daniel B. Curtis [a,b,1], Courtney D. Hatch [a,b], Christa A. Hasenkopf [b,c], Owen B. Toon [c,d], Margaret A. Tolbert [a,b,*], Christopher P. McKay [e], Bishun N. Khare [e]

[a] *Department of Chemistry and Biochemistry, University of Colorado, Boulder, CO 80309, USA*
[b] *Cooperative Institute for Research in Environmental Sciences, University of Colorado, Boulder, CO 80309, USA*
[c] *Department of Atmospheric and Oceanic Sciences, University of Colorado, Boulder, CO 80309, USA*
[d] *Laboratory for Atmospheric and Space Physics, University of Colorado, Boulder, CO 80309, USA*
[e] *Space Science Division, NASA Ames Research Center, Moffett Field, CA 94035, USA*

Received 8 August 2007; revised 4 February 2008

Available online 29 February 2008

Abstract

Titan, Saturn's largest moon, has a thick nitrogen/methane atmosphere. The temperature and pressure conditions in Titan's atmosphere are such that the methane vapor should condense near the tropopause to form clouds. Several ground-based measurements have observed sparse cloud-like features in Titan's atmosphere, while the Cassini mission to Saturn has provided large scale images of the clouds. However, Titan's cloud formation conditions remain poorly constrained. Heterogeneous nucleation (from the vapor phase onto a solid or liquid aerosol surface) greatly enhances cloud formation relative to homogeneous nucleation. In order to elucidate the cloud formation mechanism near the tropopause, we have performed laboratory measurements of the adsorption of methane and ethane onto solid organic particles (tholins) representative of Titan's photochemical haze. We find that monolayers of methane adsorb onto tholin particles at saturation ratios less than unity. We also find that solid methane nucleates onto the adsorbed methane at a saturation ratio of $S = 1.07 \pm 0.008$. This implies that Titan's methane clouds should form easily. This is consistent with recent measurements of the column of methane ruling out excessive methane supersaturation. In addition, we find ethane adsorbs onto tholin particles in a metastable phase prior to nucleation. However, ethane nucleation onto the adsorbed ethane occurs at a relatively high saturation ratio of $S = 1.36 \pm 0.08$. These findings are consistent with the recent report of polar ethane clouds in Titan's lower stratosphere.

Keywords: Titan; Atmospheres, chemistry; Ices, IR spectroscopy; Organic chemistry

1. Introduction

Titan, Saturn's largest moon, has a thick N_2/CH_4 atmosphere with methane present at 5% at the surface, remaining constant to approximately 8 km and then falling off to 1.4% in the stratosphere (Niemann et al., 2005). These measurements were made during the single Huygens Probe descent near Titan's equator and concentrations may vary with position or time. Photolysis of methane high in Titan's atmosphere produces many larger hydrocarbons and nitriles, of which ethane is the most abundant, present at ~20 parts per million by volume (ppmv) (Flasar et al., 2005; Hanel et al., 1981). Photochemistry, as well as the impact of energetic electrons, in Titan's atmosphere produces an organic haze composed of C, H, and N atoms. This solid haze material forms at altitudes near 300 km, and is thought to settle or be transported by winds towards Titan's surface. A recent study suggests the haze source is chemistry at even higher altitudes near 1000 km (Waite et al., 2007). This haze material can act as a nucleus for the condensation of organic vapors in Titan's stratosphere and troposphere. The methane vapor is likely near saturation with respect to condensation near Titan's tropopause at an altitude of ~40 km. Indeed,

* Corresponding author at: CIRES, Campus Box 216, CIRES Bldg. Rm. 318, University of Colorado, Boulder, CO 80309, USA. Fax: +1 303 492 1149.
E-mail address: tolbert@cires.colorado.edu (M.A. Tolbert).
[1] Now at: University of California, Los Angeles, Department of Atmospheric and Oceanic Sciences, Box 951565, Los Angeles, CA 90095-1565, USA.

0019-1035/$ – see front matter
doi:10.1016/j.icarus.2008.02.003

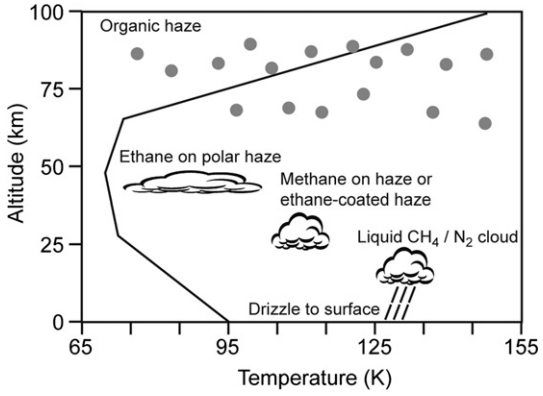

Fig. 1. Schematic diagram of possible cloud formation mechanisms in Titan's atmosphere. The solid line corresponds to Titan's temperature profile. Ethane clouds could form directly on Titan's organic haze particles as they fall from above. Methane could also condense on organic particles or form on haze particles that have been previously coated with ethane. As suggested by Tokano et al. (2006), sedimentation of the methane clouds to lower altitudes and warmer temperatures could cause melting of the particles to liquid CH_4/N_2 clouds that could drizzle to the surface.

clouds have been observed in Earth-based images, probably composed of methane (Brown et al., 2002; Griffith et al., 1998, 2000). More recently, Cassini has provided stunning global images of clouds in Titan's atmosphere and has used the movements of the cloud fields to infer dynamic information (Porco et al., 2005). Despite the now firm knowledge that several cloud types occur on Titan, the mechanism producing these clouds remains poorly understood (Barth and Toon, 2004). Fig. 1 illustrates several possible sequences of events leading to cloud formation on Titan. As methane becomes saturated near Titan's tropopause, it may condense directly onto the haze material. Alternatively, some tholins, formed at high altitude may become coated with organic vapors near the tropopause. Methane may then condense on haze material that has been coated previously (most likely by ethane). Once formed the methane particles may precipitate to lower altitudes. Depending on conditions, the clouds may evaporate, or may melt to form binary liquid CH_4/N_2 clouds (Tokano et al., 2006) that can lead to methane drizzle to the ground. Descent Imager/Spectral Radiometer (DISR) images of the Titan surface are consistent with rainfall drainage channels with organic haze collecting in the channels (Tomasko et al., 2005). Condensed methane at the surface was also implied by GC/MS data at the Huygens landing site (Niemann et al., 2005). While an ocean on Titan has been ruled out (West et al., 2005), recent observations have indicated hydrocarbon lakes on Titan (Stofan et al., 2007) and calculations suggest that evaporation from such lakes could maintain the high methane RH observed (Mitri et al., 2007).

Prior to nucleation, methane may adsorb onto the haze particles in monolayer amounts. Previous studies have shown that methane adsorbs onto surfaces of water ice (Legagneaux et al., 2002) and graphite (Inaba et al., 1986; Lysek et al., 1992) before nucleation, and that this adsorption tends to follow a Brunauer–Emmett–Teller adsorption isotherm (Legagneaux et al., 2002), a multilayer extension of the Langmuir adsorption model. A description of the Langmuir adsorption isotherm is given in Section 3 below. The adsorption process, if it occurs easily onto Titan's haze particles, could provide another mechanism for Titan's cloud formation. In this case, methane cloud nucleation would occur onto the adsorbed methane to form methane cloud particles.

In addition to methane clouds, recent observations by the Visual and Infrared Mapping Spectrometer (VIMS) aboard the Cassini spacecraft indicate the presence of a northern polar latitude cloud, with properties consistent with those expected for an ethane cloud (Griffith et al., 2006). The proposal that the clouds are ethane is partially derived from the particle size, which matches that predicted in a microphysical model of Titan's ethane cloud properties (Barth and Toon, 2003), which is in turn based on preliminary laboratory measurements from this study. As in the case of methane, ethane may adsorb onto the haze particles in monolayer amounts prior to nucleation. The adsorption process and subsequent nucleation could provide the mechanism for the formation of Titan's observed ethane clouds.

To study Titan cloud formation near the tropopause, we have performed laboratory studies of methane and ethane adsorption and nucleation onto organic particles (tholins) representative of Titan's haze particles. We find that methane adsorbs onto the tholin particles following a Langmuir isotherm. We find that nucleation of solid methane on the methane-coated particles occurs at a critical saturation ratio of $S_{crit} = P(CH_4)/VP(CH_4) = 1.07 \pm 0.008$, where $P(CH_4)$ is the ambient pressure of methane and $VP(CH_4)$ is the vapor pressure of methane as a function of temperature. Further, we find that methane nucleation on a range of other substrates including ethane occurs at a low supersaturation, presumably due to the ease of methane adsorption. These low values of S_{crit} imply that methane cloud formation in Titan's atmosphere will occur with relative ease. We also examine nucleation of ethane onto tholins. We find that ethane adsorbs onto tholin particles prior to nucleation. However the phase of the adsorbed ethane differs from that of bulk stable phase II ethane. We thus find that ethane nucleation onto adsorbed ethane occurs at a relatively high value of $S_{crit} = 1.36 \pm 0.08$.

2. Experimental

2.1. Haze analog production and particle size determination

We have formed an organic haze material (tholin), which resembles Titan's haze using an AC current crossing a gap between two electrodes inside a glass reaction vessel. This technique has been used for the production of tholin for over a decade (McKay, 1996). It has been shown that this material matches the optical properties of Titan's haze (Khare et al., 1984). The apparatus used in this experiment was described previously (Curtis et al., 2005) and is summarized here only briefly.

The glass reaction vessel was constructed containing two tungsten electrodes piercing the glass walls and converging at the center of the vessel, with a gap between them of ~1 cm. The vessel is 25 cm in length and 6 cm inside diameter (~700 cm^3 in volume) and is equipped with a Viton O-ring which allows

the vessel to be opened and objects placed inside. For this study a silicon wafer with a diameter of 2.5 cm was placed in the bottom of the vessel for deposition of the tholin particles. The reaction vessel was evacuated to a pressure of ∼20 mTorr using a mechanical pump, then filled with a gas mixture composed of 90.00% N_2 and 10.00% CH_4 (Research Grade, Airgas Intermountain) until a pressure of 300 ± 50 Torr was reached, as monitored by a Convectron Pirani thermal conduction pressure gauge (Granville–Phillips). The vessel was then isolated from the pump and the gas mixture was exposed to a spark discharge from a hand-held high frequency generator, or Tesla coil (Fisher Scientific). The spark discharge is an AC current with a frequency of 500 kHz and a voltage across the electrode gap of approximately 10,000 V. The silicon wafer rested directly underneath the gap between the electrodes, which facilitated an evenly distributed deposition of the particles onto the silicon wafer. The gas mixture was flushed out and replaced each hour. After 24 h, the wafer was flipped to expose its other side. This process was continued until each side of the wafer had been exposed for 24 h, for a total exposure time of 48 h. Based on previous scanning electron microscope images from Curtis et al. (2005) the particle film on the wafer is found to be a collection of aggregated particles on the surface, covering the wafer with at least several monolayers of particles. The particles on the surface retain certain characteristics, such as size and curvature, which should allow them to act as condensation nuclei in a manner consistent with that of individual suspended particles. In addition, as described later, we find that the nucleation of gases onto the particles does not match the nucleation of gases onto a bare silicon wafer, indicating that the silicon wafer itself does not interfere with the measurement of nucleation onto the particles.

The empirical formula of the tholin film prepared in this manner (C_5H_5N) was reported earlier (Curtis et al., 2005). The infrared spectra of the haze has also been published previously (Curtis et al., 2005) and is consistent with infrared spectra reported for tholins by others (Khare et al., 1984; McKay, 1996).

The particle sizes in the present study were determined using a scanning particle mobility sizer (SMPS). The SMPS consists of a TSI Model 3080 Electrostatic Classifier with a Model 3081 Differential Mobility Analyzer (DMA) and a Condensation Particle Counter (CPC). The DMA applies an electric field to a flow of charged, polydispersed aerosols and selects particles by size based on electrical mobility against the drag force of the sheath flow. The monodispersed particles are then flowed into the CPC, which counts each particle by light scattering. For the particle size determination, a 10% CH_4 in N_2 gas mixture at 612 Torr was exposed to the Tesla coil in a flow system operating under slow flow conditions of 30 sccm (standard cubic centimeters per minute). After particle formation, nitrogen was added for a total flow of 0.3 L min^{-1} for proper function of the SMPS system. Particle size distributions for the experiment are shown in Fig. 2. It can be seen in the top panel of Fig. 2 that the particles follow a roughly lognormal distribution with a mode diameter of 162 nm. Transmission Electron Microscope images of the collected tholin particles under the exact experimental conditions were also obtained. Fig. 3 shows a sample TEM image. In this image, it can be seen that the tholin particles are spherical, with a range of particle sizes below 1 μm. The TEM images are thus consistent with the sizes determined from the SMPS system. Below, the size distributions in Fig. 2 will be used to determine the surface area of the particles and hence allow estimation of the surface coverage of methane and ethane on the tholin particles.

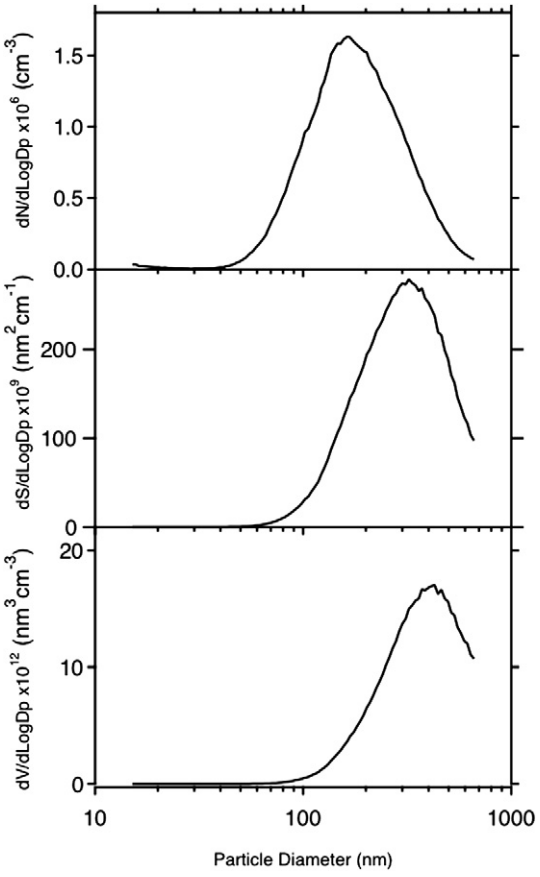

Fig. 2. The size distribution of the tholin particles produced in this study, as measured using a commercially available SMPS instrument. The three panels from top to bottom correspond to the number-, surface area-, and volume-weighted size distributions.

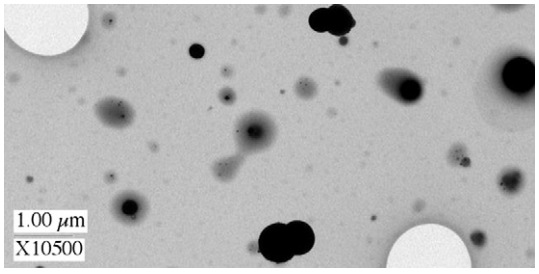

Fig. 3. A representative transmission electron microscope image of the tholin particles produced in this study. The solid tholin particles are black in the image. The lighter gray area that surrounds some of the particles is believed to be due to liquid-like regions. The large white circles are bubbles in the film coating the TEM grid. The solid black line beneath the white box labeled "1.00 μm" in the lower left corner is one micron in length.

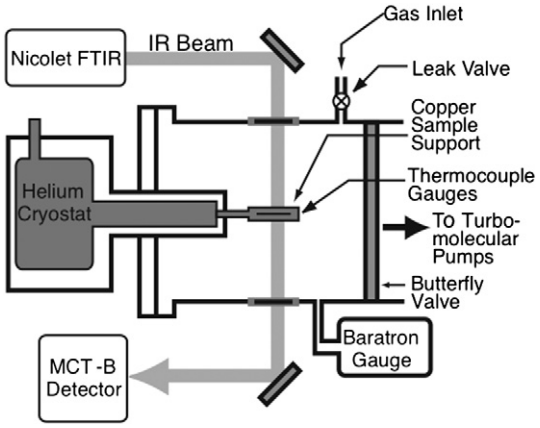

Fig. 4. Experimental apparatus. The apparatus was described in detail previously (Curtis et al., 2005) and consists of a stainless steel vacuum chamber and cold cryostat arm monitored with transmission FTIR spectroscopy.

2.2. Adsorption and nucleation experiments

Adsorption and nucleation experiments were performed in a stainless steel vacuum chamber shown schematically in Fig. 4. The particle-coated silicon wafer was transferred from the glass reaction vessel to the vacuum chamber in room air conditions, with the wafer being exposed to room air for a period of approximately five minutes. The chamber is equipped with a leak valve for the introduction of methane gas, an MKS Baratron capacitance manometer gauge to monitor the pressure of the introduced gas and a Fourier Transform Infrared (FTIR) spectrometer to measure the composition of the condensed phase. The temperature of the silicon wafer was controlled through a combination of compressed helium cooling (Helium Compressor: APD Cryogenics, Model HC-4MK2-1; Cryostat Expander: Advanced Research Systems, Model DE-204B) and resistive heating, and was monitored by a silicon diode. The walls of the chamber were at room-temperature, while the cooling arm of the cryostat was maintained at a slightly higher temperature than the silicon wafer, such that the silicon wafer was the coldest point in the chamber. Based on previous measurements in Curtis et al. (2005), the thermal conductivity of the copper mount and silicon wafer allow for very small variations in temperature across the silicon wafer on the order of ± 0.1 K. Also as described in Curtis et al. (2005), a distinct advantage of this experimental technique is that the accuracy of the temperature measurement is not critical due to the nature of the measurement. However, we estimate that the accuracy of the temperature measurement is ± 1.5 K. Methane nucleation experiments were performed on either the blank silicon wafer, the wafer coated with tholin particles, or the silicon wafer coated with solid ethane or water ice films. Ethane nucleation onto a silicon wafer coated with tholin particles and water ice films was also probed.

In a typical experiment, the chamber was first evacuated to a pressure of approximately 1×10^{-7} Torr and the temperature lowered. Methane nucleation experiments were performed over a temperature range of 41.0–49.0 K with no difference in results observed over the range of temperatures. Experiments at the higher temperatures found in Titan's atmosphere were not possible in our system because we could not maintain high enough pressures of methane. Based on the lack of temperature dependence over the range 41.0–49.0 K, we presume that our results will be valid at Titan-like temperatures. Methane vapor was introduced into the chamber via a leak valve and the pressure was increased incrementally by approximately 0.01–0.02 mTorr every 30 s. Adsorption of methane onto the tholin particles was noted by a very slight increase in the infrared absorbance of the methane stretching and bending mode peaks at 3000 and 1300 cm^{-1}, respectively. This adsorption occurred prior to nucleation, and could be observed due to the high surface area of the tholin particles present on the silicon wafer that allowed for a significant mass of adsorbed methane to be present on the tholin.

The nucleation point was then determined by a very large increase in the methane infrared absorbance with an incremental addition of methane. The nucleation pressure was typically 0.05–3 mTorr depending on the temperature and the supersaturation required. When nucleation occurred, it was detected very rapidly (within four seconds, the time resolution of the FTIR) as a sharp increase in the methane absorption features in the FTIR spectrum and a sharp drop in the pressure in the chamber pressure.

After nucleation and growth of the methane film, a frost point calibration was performed. The pressure in the chamber was adjusted until the condensed methane film was neither growing nor desorbing as determined from the strength of the methane infrared absorption features. By definition, this is the vapor pressure of the methane film. The critical saturation ratio, S_{crit}, was determined by dividing the pressure in the chamber at the point of nucleation by the measured vapor pressure.

In addition to studies of methane, the adsorption and nucleation of ethane onto tholin material was also studied. The experimental protocol was the same as in the methane experiments except that the temperatures were around 75 K. A previous study probed the nucleation of butane on tholin material and several organic films (Curtis et al., 2005).

3. Results

3.1. Methane adsorption/nucleation on tholins

Fig. 5 shows infrared spectra collected during a typical experiment for methane adsorption and nucleation onto tholin particles. The spectra shown are the ratio of the absorbance to a background spectrum of the tholin particles. The spectra indicate nucleation of phase I methane, the stable crystalline phase of methane above 20 K (Signorell and Jetzki, 2007). The inset shows detailed views of the methane peak at 1300 cm^{-1} during the adsorption process. The spectra in the inset have been offset for clarity and correspond to 0, 100, 500, and 800 s from bottom to top. The strongly absorbing spectrum in the main panel shows nucleated methane on the tholin material at 2300 s. The sloping background in the spectrum obtained at 2300 s is due to Mie scattering by the particles as they grow due to methane condensation.

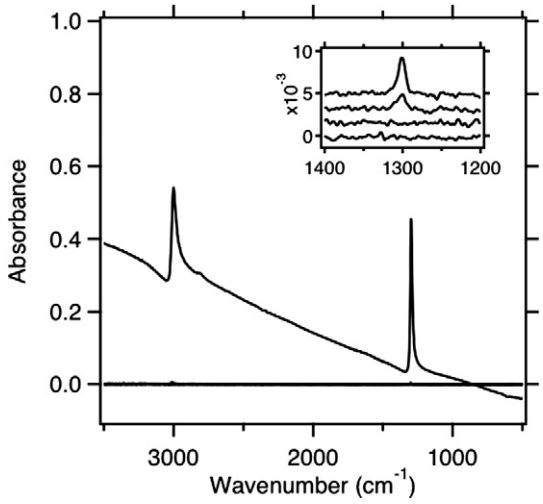

Fig. 5. Solid methane spectra as measured in this study (ratioed to the bare tholin sample). The spectra shown in the main panel were collected at $t = 0$ and 2300 s. The latter corresponds to a film of solid methane nucleated onto the tholin material. The inset shows spectra collected at 0, 100, 500 and 800 s and shows evidence for the adsorption of methane onto the tholin material prior to nucleation. The inset spectra have been offset for clarity and show the detail of the methane bending mode at 1300 cm^{-1}. The spectra collected at 500 s and 800 s clearly indicate methane adsorbed onto the tholin material prior to nucleation.

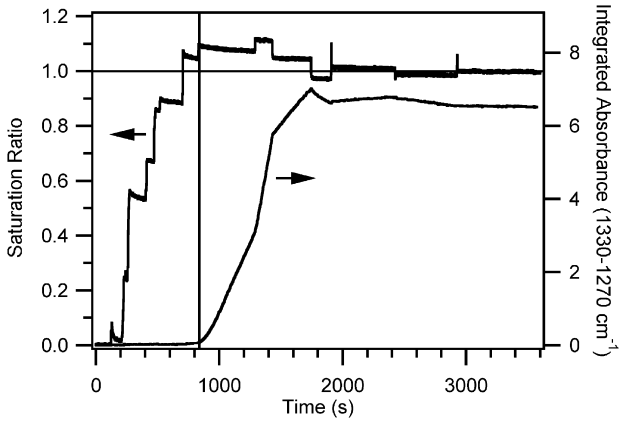

Fig. 6. Example experiment for methane adsorption/nucleation on tholins. This plot shows the saturation ratio of methane vapor in the chamber (left axis) and the integrated absorbance of the methyl rocking mode (right axis) versus time. It can be seen that as the saturation ratio is increased, methane nucleation onto the tholin particles is observed when the integrated absorbance increases suddenly at $t = 850$ s and a critical saturation ratio of $S_{crit} = 1.07$. In addition, a very slight increase in the integrated absorbance is observed prior to nucleation. We attribute this slight increase to methane adsorption onto the tholin surface prior to nucleation, which is observable due to the high surface area of the tholin film.

The peak intensity of the 1300 cm^{-1} peak is used to construct a time series of methane adsorption, shown in Fig. 6. Also shown in Fig. 6 is the saturation ratio of methane during the experiment. It can be seen that at time $t = 40$ s, prior to the introduction of methane vapor to the chamber, no methane had condensed onto the tholin particles. As time continued during the experiment, methane vapor was introduced into the chamber incrementally, as seen in Fig. 6 by the increase in saturation ratio, plotted on the left axis. After the saturation ratio reached a critical value (S_{crit}), nucleation of methane vapor was seen as a sharp increase in the integrated absorbance of the methane bending mode plotted on the right axis, as shown in Fig. 6. The value of the saturation ratio when the methane film begins to nucleate, as seen by the sharp increase in the integrated absorbance at $t = 850$ s, is defined to be the critical saturation ratio, S_{crit}. In the example experiment, the critical saturation ratio for methane vapor nucleating onto adsorbed methane was found to have a value of $S_{crit} = 1.10$. After nucleation a frost point calibration was performed as described above and previously (Curtis et al., 2005).

Prior to the pressure reaching a saturation ratio of $S = 1$, a slight increase in the methane stretching and bending modes was noted, as shown in the inset in Fig. 5. The spectra at 0 and 100 s (the lower two spectra shown in the inset) show that no adsorbed methane is initially present. However, the upper two spectra, taken at 500 and 800 s show that methane has adsorbed onto the tholin material prior to nucleation because the methane absorption band is present. The absorbance is stronger at the higher saturation ratio present at 800 s. We attribute this slight increase in the absorbance to the adsorption of methane vapor onto the surface of the tholin particles prior to achieving a saturation ratio of $S = 1$. This absorbance is observable due to the relatively high surface area of the tholin particle film.

Using the peak height of the methane bending mode at 1300 cm^{-1}, an adsorption isotherm was constructed. Fig. 7 shows the peak height of the methane bending mode at 1300 cm^{-1} plotted versus the saturation ratio of methane vapor in the chamber. The methane adsorption onto the surface of the tholin particles was modeled using the Langmuir adsorption isotherm:

$$\theta/\theta_{max} = (b^* P)/(1 + b^* P), \quad (1)$$

where θ/θ_{max} is the fractional coverage of the surface by methane, b is a constant determined from the fit, and P is the pressure of methane in the chamber. For Langmuir adsorption, the coverage is expected to increase linearly with pressure at low pressures, then saturate at monolayer coverage for higher pressure. The data in Fig. 7 is fit to the Langmuir expression and the fit is shown as the solid line. The best fit is obtained using $b = 14071 \pm 682$ Torr^{-1} and a maximum peak height of 0.0137 absorption units. Thus at the plateau level in Fig. 7, the coverage θ/θ_{max} is approximately 0.75. For the plot shown in Fig. 7, Eq. (1) has been cast in terms of the saturation ratio by dividing the numerator and denominator by the vapor pressure of methane at 45 K, 1.576×10^{-4} Torr (Moses et al., 1992).

The Langmuir model assumes that the maximum coverage at saturation is one monolayer. To independently determine the methane coverage at saturation, we have used infrared spectroscopy to quantify both the tholin and methane masses. We have also measured the tholin mass directly for comparison with that determined spectroscopically. To obtain a measurable amount of tholin particles, we continued particle production for 75 h. After this time, a measurable mass was obtained using an analytical balance. After scaling to the exposed area of the silicon wafer in the vacuum chamber, 1.57 cm^2, and the exposure time of the samples used in our experiments (48 h), we find a

tholin mass of 1.6×10^{-4} g for the conditions of our experiment.

The second method for determining the mass of tholin particles available for CH_4 adsorption involved treating the particles as a thin film and quantification by FT-IR spectroscopy. Using the peak height at 1581 cm^{-1} and the optical constants for tholins reported by Khare et al. (1984), the mass of tholin particles was determined by first converting the imaginary refractive index for tholin at 1581 cm^{-1} to an absorption coefficient using:

$$\alpha = 4\pi k \nu, \tag{2}$$

where ν is the peak position (cm^{-1}), k is the dimensionless imaginary refractive index and α is the base e absorption coefficient (cm^{-1}). The absorption coefficient was then divided by the density of tholin particles, 0.8 g/cm^3 (Trainer et al., 2006), to determine an absorption cross section, a (cm^2/g). Beer's law was then used to determine the mass of tholin particles probed by the area of the IR beam, m_{probed}, g/cm^2_{probed} as follows:

$$am_{\text{probed}} = \ln 10^A, \tag{3}$$

where A is the base 10 absorbance. Using this method, we find 9.3×10^{-5} g/cm^2_{probed} of tholin particles probed by the IR beam. Upon scaling this value to the exposed geometric surface area of the silicon wafer in the vacuum chamber, 1.57 cm^2, we find an exposed tholin mass of 1.46×10^{-4} g, in excellent agreement with the value obtained by weighing.

The same method used to determine the mass of tholin by FT-IR spectroscopy was used to obtain the mass of CH_4 adsorbed to the surface of the tholin particles. Using the density and optical constants for crystalline CH_4 (Moses et al., 1992; Pearl et al., 1991), the mass of adsorbed CH_4 probed by the area of the IR beam was determined. The mass of adsorbed CH_4 at the plateau region of Fig. 7 (3.2×10^{-7} g/cm^2) scaled to the surface area of the silicon wafer, 1.57 cm^2, results in 5×10^{-7} g CH_4 adsorbed to the tholin particles at saturation. Thus, at saturation, we find that there is approximately 0.3% CH_4 by mass adsorbed to the tholin particles.

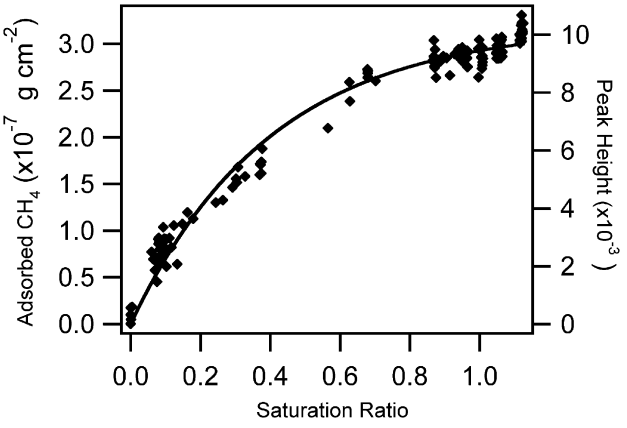

Fig. 7. Observed and modeled adsorption isotherm for methane adsorption onto tholin particles. The plot shows the mass of adsorbed methane on the left axis and the corresponding peak height for the methane bending mode feature at 1300 cm^{-1} on the right axis. Both are plotted as a function of saturation ratio. It can be seen that methane adsorbs onto the tholin film prior to nucleation (which occurs at a saturation ratio of $S = 1.07$ on average). Also shown is a model calculation of the Langmuir isotherm for methane adsorption onto the tholin film which closely follows the measured data.

To convert the adsorbed mass to coverage on the particles, the particle surface area density is needed. The size distribution data in Fig. 2 allow determination of the ratio of surface area to volume for the tholin particles. The surface to volume ratio was found to be 2.2×10^5 ($\pm 1.3 \times 10^5$) cm^2/cm^3. Using this value, an adsorbed mass of 0.3% CH_4 by mass, a tholin density of 0.8 g/cm^3 (Trainer et al., 2006) and the molecular weight of CH_4 of 16 g/mol, the saturation coverage of CH_4 on tholin particles is estimated to be 4.1×10^{14} molecules/cm^2. This value is on the order of a monolayer (or a bit less) and agrees well with the Langmuir model showing $\theta/\theta_{\max}$ of approximately 0.75 just prior to nucleation. Thus methane appears to adsorb to near monolayer coverage at a saturation ratio near unity.

3.2. Methane adsorption on other surfaces

Because higher-order hydrocarbons have a lower vapor pressure, it is possible that they will condense on the tholins at a higher altitude in Titan's atmosphere and then methane would nucleate on hydrocarbon-coated tholins. To probe the effect of an ethane substrate, we measured methane nucleation on ethane, the second most abundant hydrocarbon in Titan's atmosphere. Fig. 8 shows infrared spectra collected during an experiment to probe methane nucleation onto a film of solid ethane. In this case, the spectra were ratioed to a spectrum of the bare silicon wafer. Spectrum A in Fig. 8 shows the blank wafer. Ethane vapor was introduced into the chamber and condensed onto the wafer as a solid film, shown in Spectrum B, which corresponds to a time of $t = 500$ s. The chamber was then evacuated and methane vapor was introduced, with the pressure increasing incrementally until methane nucleation occurred. Spectrum C in Fig. 8 shows the methane film condensed on the ethane film, as can be seen by the methane peaks at 1300 and 3010 cm^{-1}. The methane band intensity at 1300 cm^{-1} as a function of methane saturation ratio for these experiments is shown in Fig. 9. Here it can be seen that methane condensation on ethane, similar to tholins, occurs very near a saturation ratio of unity. The value determined in this experiment was $S_{\text{crit}} = 1.10 \pm 0.007$.

A comparison of all the values of S_{crit} determined in this work for methane nucleation, along with the corresponding standard deviations is given in Table 1. In addition to ethane and tholins, methane nucleation was also studied on water ice and a bare silicon wafer.

Table 1
Methane nucleation results

Substrate	T (K)	No. of experiments	Avg. S_{crit}	Standard dev.
Tholin	45	5	1.07	0.008
Ethane	45	6	1.10	0.007
Ethane	47	5	1.09	0.023
Si	45	4	1.14	0.052
Ice grown at 160 K	45	4	1.14	0.057

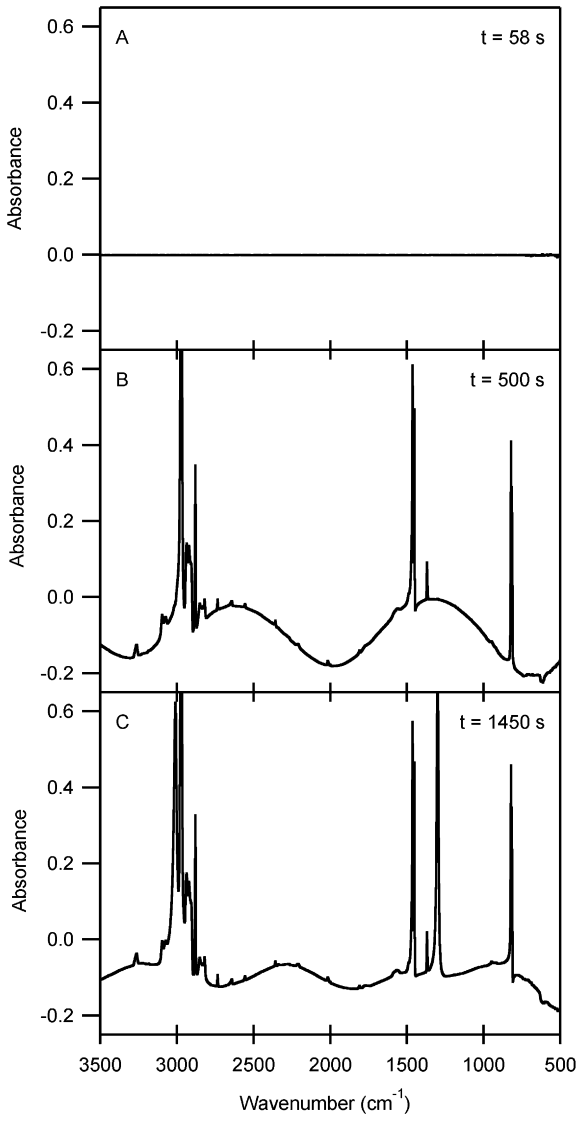

Fig. 8. Infrared absorbance of methane peaks during adsorption of methane on ethane. The spectra are ratioed to the bare silicon wafer and the time values correspond to the experiment shown in Fig. 9. At 58 s, the wafer is still bare while an ethane film is condensed at 500 s. At 1450 s, a methane film has grown on the ethane film. The ethane film was extremely stable after growth due to the very low vapor pressure of ethane at the temperature of the wafer. Tests were performed where the chamber was evacuated with the ethane film on the wafer and no loss of ethane was observed over periods of approximately one hour. In a typical methane nucleation on ethane film experiment, the chamber was evacuated for periods of 5–10 min prior to the introduction of methane to the chamber.

It can be seen in Table 1 that within experimental error, methane nucleation onto tholin particles, ethane, bare silicon, and water ice occurs at the same critical saturation ratio, very near a value of unity. We propose that the consistency in the methane nucleation results is due to the fact that methane adsorbs onto each of these surfaces prior to nucleation, then nucleates on itself to grow into a film. We were able to measure this adsorption on a film of tholin particles due to the high surface area of the tholin film. We cannot directly measure methane adsorption onto the relatively low surface areas of silicon, ethane, and water ice, but presume it is occurring.

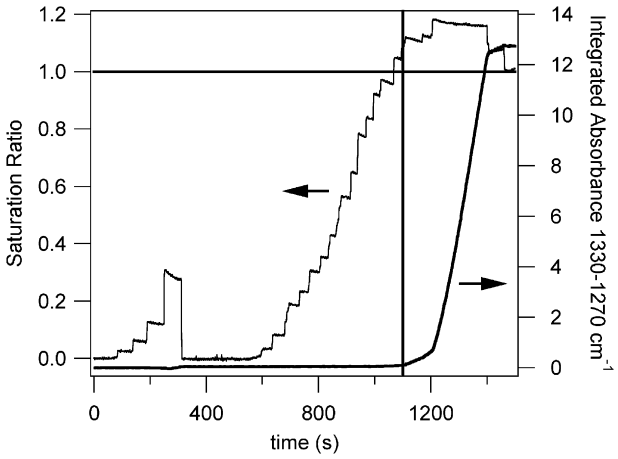

Fig. 9. Example experiment for methane nucleation onto a film of solid ethane. Saturation ratio for methane (left axis) and the integrated absorbance of the methane bending mode (right axis) are shown versus time. An ethane film is grown between 150 and 350 s, and thus the rise in pressure during that time period is due to ethane and not methane. It can be seen that methane nucleates onto ethane at a saturation ratio of $S = 1.10$.

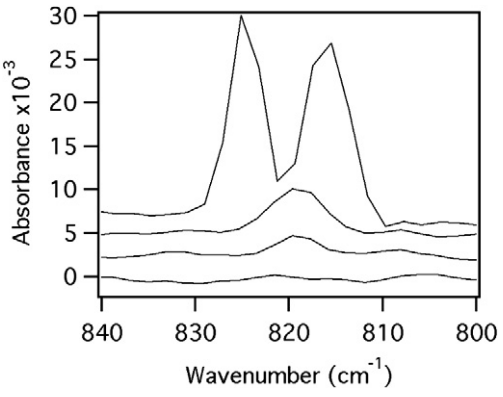

Fig. 10. Infrared spectra of ethane adsorption and nucleation onto tholin particles, referenced to a spectrum of the bare tholin particles. From bottom, the spectra were collected at saturation ratios of $S = 0.882$, 1.18, 1.38, and 1.36. Nucleation in this experiment occurred at $S = 1.38$, after which the film started growing and the pressure dropped. The top spectrum is representative of bulk stable phase II ethane.

3.3. Ethane nucleation on tholins

In addition to methane nucleation, ethane adsorption and nucleation on tholin particles was also studied. Fig. 10 shows infrared spectra collected during a typical experiment for ethane adsorption and nucleation onto tholin particles. As in Fig. 5, the spectra shown are the ratio of the absorbance to a background spectrum of the tholin particles. However, here a detailed view of the region between 810 and 830 cm^{-1} is shown, corresponding to the ν_9 ethane vibration, a CH_3 rocking mode. The spectra have been offset for clarity and correspond to increasing saturation ratio from $S = 0.88$ in the bottom spectrum to $S = 1.36$ in the top. Initially, the mode appears as a single band centered at 820 cm^{-1}. However, at higher saturation ratios (after nucleation), the ethane band forms the doublet characteristic of the stable phase II ethane (Pearl et al., 1991).

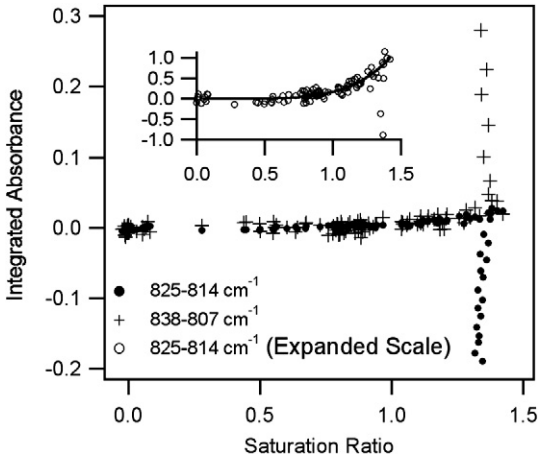

Fig. 11. Ethane adsorption and nucleation on tholin particles. The plus symbols show the integrated absorbance from 807 to 838 cm^{-1} as a function of saturation ratio. Ethane nucleation is indicated by the sharp rise in integrated absorbance at $S = 1.38$. The closed circles representing the integrated absorbance from 814 to 825 cm^{-1} show ethane adsorption into a metastable phase. The inset shows ethane adsorbing prior to nucleation. The data in the inset has been normalized to allow for the plot of an adsorption isotherm, shown as a solid line. Nucleation is observed by a sharp decrease in this band as metastable ethane converts to stable phase II ethane.

The evolution of the spectra with increasing saturation ratio can be used to gain insight into the adsorption and nucleation processes. Fig. 11 shows the integrated intensity of the entire band from 807 to 838 cm^{-1} as a function of S as the plus symbols. Here it can be seen that the integrated absorbance increases sharply at $S = 1.38$, characteristic of nucleation. In contrast, when only the band area from 814 to 825 cm^{-1} is integrated (encompassing the adsorbed ethane peak), the plot in Fig. 11 (circles) is obtained. Here it can be seen that ethane is steadily adsorbing onto the tholin particles as the saturation ratio is raised above unity. At nucleation, however, there is a sharp *decrease* in intensity of this band as the adsorbed ethane in one phase nucleates to the stable phase II ethane.

The inset of Fig. 11 shows an expanded view of the ethane adsorption prior to nucleation. By comparison with Fig. 7, it can be seen that the ethane adsorption does not follow a Langmuir type adsorption. Instead the graph is more similar to water uptake curves observed frequently for Earth aerosols composed of low-solubility organics where water begins to be taken up near saturation (Garland et al., 2005). In the ethane case, it appears that a metastable phase of ethane adsorbs to the tholins near saturation, followed by nucleation at $S = 1.38$. Because optical constants for adsorbed ethane are not available, we use the optical constants of Pearl et al. (1991) for the ν_9 transition in ethane II and assume the transition strength is similar for the same band in adsorbed ethane. With this assumption, we can then roughly estimate the amount of ethane adsorbed just prior to nucleation. Assuming the surface area of the tholin particles is 2.2×10^5 cm^2/cm^3 as determined above, a molecular weight of 30 g/mole for ethane and a density of ethane at 77 K of 0.713 g/cm^3 (Moses et al., 1992), the coverage just prior to nucleation at $S = 1.38$ is 4.9×10^{14} molecules/cm^2, or approximately one monolayer.

Table 2
Ethane nucleation results

Substrate	T (K)	No. of experiments	Avg. S_{crit}	Standard dev.
Tholin	75	4	1.36	0.080
Ice grown at 160 K	72–74	7	1.46	0.180

Thus, both methane and ethane appear to adsorb to the tholin particles prior to nucleation. However, in contrast to methane adsorption, the ethane adsorbs in a configuration that gives a unique spectral signature that is quite different from bulk ethane. Further, nucleation of ethane on the adsorbed ethane does not occur until a relatively high saturation ratio near $S_{crit} = 1.36 \pm 0.080$ on average, as shown in Table 2.

4. Discussion

Some adsorbing molecules are said to wet the substrate, leading to multilayer adsorption and growth near $S = 1$. If the material wets the substrate, nucleation does not need to occur for growth to proceed. Methane has been shown to wet the surface of some materials such as graphite (Inaba et al., 1986). However, with tholins we find the adsorption follows a Langmuir isotherm, which is characteristic of monolayer adsorption. We also find nucleation occurs at a saturation ratio of $S = 1.07 \pm 0.008$. Within error, growth of the methane films may be occurring at $S = 1$. Alternatively, a nucleation event is occurring which requires a critical saturation ratio slightly greater than unity.

We are only able to observe adsorption for methane onto the tholin particles because of the very high surface area of that substrate, but presumably adsorption of methane is occurring on all substrates. The critical saturation ratio for methane nucleation onto tholin particles was identical within experimental error to the critical saturation ratio for methane nucleation onto other substrates studied, including a blank silicon wafer, ethane and water ice. Methane has been observed to adsorb onto various substrates (Inaba et al., 1986; Legagneaux et al., 2002; Lysek et al., 1992). Therefore, the critical saturation ratio measured in this study is that required for solid methane to nucleate onto adsorbed methane molecules on the surface of the substrate.

Curtis et al. (2005) found that butane would nucleate on tholin particles at a critical saturation ratio of $S_{crit} = 1.30 \pm 0.06$, while butane nucleation on ice required $S_{crit} = 1.59 \pm 0.12$, and butane nucleation on hexane and acetonitrile required $S_{crit} = 1.36 \pm 0.11$ and $S_{crit} = 1.13 \pm 0.06$, respectively. Thus butane appears to act differently than methane by having a larger S_{crit} that varies according to the substrate. Fig. 12 shows the integrated absorbance of the bending mode peak for methane and ethane (measured in this study) and butane (measured in Curtis et al., 2005) versus saturation ratio for adsorption onto a tholin particle film. It can be seen that methane growth occurs at a substantially lower value of S_{crit} than does ethane or butane.

Like methane, ethane adsorbs onto a tholin particle film prior to nucleation, but in this case nucleation occurs at a relatively

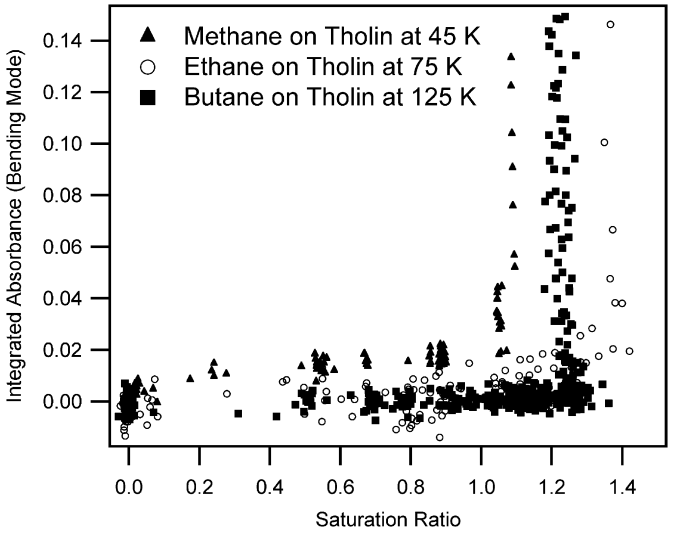

Fig. 12. Methane and ethane nucleation contrasted with butane nucleation. This plot shows the integrated absorbance of the methane bending mode, and ethane and butane rocking modes vs saturation ratio for nucleation on tholins. It can be seen that methane and ethane adsorb onto the tholin material prior to nucleation at a saturation ratio of $S = 1.07$ and 1.36, respectively on average. In addition, it can be seen that butane does not adsorb in a measurable amount prior to nucleation, and that butane nucleation occurs at a saturation ratio of $S = 1.25$ in this example (1.30 on average) (Curtis et al., 2005).

high critical saturation ratio of $S_{crit} = 1.36 \pm 0.08$, somewhat higher than that required for butane nucleation. Based on the infrared spectra, the adsorbed ethane is in a different configuration than the stable bulk solid ethane (phase II) at the temperatures studied. Thus, a higher critical saturation ratio may result due to a relatively high strain between the adsorbed and bulk ethane.

A possible explanation of the difference in behavior between methane and ethane nucleation lies in differences in surface adsorption. Previous studies of ethane adsorption onto graphite have shown that at monolayer coverage, ethane molecules stand on end with their C–C axis perpendicular to the graphite plane (Jain et al., 1994). This arrangement may not provide the best match for bulk ethane nucleation. Alternatively, the adsorbed ethane may be in an amorphous state that does not provide a good match for phase II ethane. Adsorption of metastable phases of nitric acid/H_2O prior to nucleation to crystalline nitric acid hydrates are well known in studies of clouds on Earth (Iraci et al., 1995; Zondlo et al., 2000; Hudson et al., 2002).

In contrast to the ethane case, when methane nucleates we are observing the spectrum of phase I (Signorell and Jetzki, 2007), the stable form under Titan conditions. In phase I methane, all of the tetrahedral methane molecules are orientationally disordered (Signorell and Jetzki, 2007), and thus nucleation of the bulk material may not be orientationally hindered.

5. Application to Titan's clouds

The relatively low critical saturation ratio measured in this study implies that solid methane will adsorb onto Titan's haze particles at supersaturations below one, and then grow at low supersaturations. Since methane will adsorb onto condensation nuclei prior to nucleation, the composition of the nuclei is likely irrelevant. Methane vapor is in contact with methane molecules already adsorbed to the surface, and thus nucleation is relatively easy, requiring at most a critical saturation ratio of only approximately $S_{crit} = 1.07 \pm 0.008$, regardless of the substrate used in this study.

In Titan's atmosphere, methane will nucleate at similar supersaturations onto bare haze material or haze material coated with solid ethane. Methane in Titan's atmosphere should thus condense easily to form clouds. These findings are in agreement with recent measurements of the methane column abundance, which indicate that methane is not excessively supersaturated in the troposphere (Tokano et al., 2006).

This study did not determine whether the S_{crit} value depends on particle radius. However, the particles produced in this study have approximately the same radius as those particles in Titan's atmosphere and the measured values for S_{crit} from this study should approximate those found in Titan's atmosphere.

Ethane is the main photochemical product of methane dissociation in Titan's atmosphere. It had been thought that accumulation of ethane over the 4.5 billion year lifetime of Titan would have led to a global ethane ocean on Titan. However, such an ocean has not been detected (West et al., 2005) leading to questions about the ultimate fate of the ethane. Recently, Hunten (2006) suggested that the ethane could be absorbed into the haze particles and thus deposited with the haze onto the surface in a solid form. Griffith et al. (2006) suggested ethane ice clouds observed at the poles during the winter might form an ethane ice cap and thus contribute to the lack of liquid ethane on the surface.

Our studies find that while ethane does readily adsorb onto the haze material, only a monolayer or less of ethane forms when the air is subsaturated with respect to ethane. For example, assuming an aggregate particle composed of 512 monomers of radius 0.05 μm (Tomasko et al., 2005) and 150 particles/cm^3 (Toon et al., 1988), we estimate that only 10^{10} molecules/cm^3 of ethane will be adsorbed to the haze compared to 5×10^{13} molecules/cm^3 ethane total at 70 km. Thus, under our conditions not enough ethane could be sequestered in the haze while it is in the atmosphere to account for a significant loss of atmospheric ethane. As suggested by Hunten (2006), it may still be possible for a significant amount of ethane to be sequestered in the cold dunes on the surface (Lorenz et al., 2006), depending on the size and surface area of the particles that comprise the dunes.

In contrast to subsaturated air, if the atmosphere becomes supersaturated, we find that ethane will condense onto the haze material. Griffith et al. (2006) suggest that the polar ethane clouds on Titan have a particle radius in the range 1–3 μm. We find a saturation ratio of $S = 1.36$ for ethane nucleation on the tholins. Following the method described in Curtis et al. (2005), we can estimate the ethane cloud particle size for different nucleation scenarios. We use a steady-state approximation in a simple one-dimensional model of a horizontal slice of Titan's atmosphere and equate the photochemical production rate of ethane by mass and the mass loss rate due to condensation

of the ethane to particles that can fall out of the layer. Assuming an ethane production rate of 2.9×10^{-13} g/cm^2 s (Barth and Toon, 2003), a tholin number density of 150/cm, a fall velocity of 50 cm s^{-1} (Toon et al., 1988) and a particle density of 0.8 g/cm^3 (Trainer et al., 2006), we estimate that the ethane cloud particles would have a radius of 0.6 μm if all of the haze particles were to nucleate. However, since we observe $S = 1.36$ for ethane on tholins, the nucleation would be more selective and fewer of the particles should nucleate an ethane cloud. For example, cirrus clouds on earth nucleate at $S = 1.5$ and only 1 in 10^4 particles nucleate a cloud. For the case of Titan with nucleation at $S = 1.36$, if 1 in 100 particles nucleated a cloud, we estimate a cloud particle radius of 1.8 μm. Thus, the selective nucleation we observe in the laboratory for ethane yields results consistent with the ethane cloud particle size of 1–3 μm proposed by Griffith et al. (2006).

Acknowledgments

D.B.C. was supported by NASA's Graduate Student Researchers Program through NASA Ames Research Center. O.B.T. was supported by NASA's Planetary Atmospheres Program NNG05GA53G. M.A.T. received partial support through NASA's Planetary Atmospheres Program through Grant NNX07AF19G.

References

Barth, E.L., Toon, O.B., 2003. Microphysical modeling of ethane ice clouds in Titan's atmosphere. Icarus 162, 94–113.

Barth, E.L., Toon, O.B., 2004. Properties of methane clouds on Titan: Results from microphysical modeling. Geophys. Res. Lett. 31. Art. No. L17S07.

Brown, M.E., Bouchez, A.H., Griffith, C.A., 2002. Direct detection of variable tropospheric clouds near Titan's south pole. Nature 420, 795–797.

Curtis, D.B., Glandorf, D.L., Toon, O.B., Tolbert, M.A., McKay, C.P., Khare, B.N., 2005. Laboratory studies of butane nucleation on organic haze particles: Application to Titan's clouds. J. Phys. Chem. A 109, 1382–1390.

Flasar, F.M., and 44 colleagues, 2005. Titan's atmospheric temperatures, winds, and composition. Science 308, 975–978.

Garland, R.M., Wise, M.E., Beaver, M.R., DeWitt, H.L., Aiken, A.C., Jimenez, J.L., Tolbert, M.A., 2005. Impact of palmitic acid coating on the water uptake and loss of ammonium sulfate particles. Atmos. Chem. Phys. 5, 1951–1961.

Griffith, C.A., Owen, T., Miller, G.A., Geballe, T., 1998. Transient clouds in Titan's lower atmosphere. Nature 395, 575–578.

Griffith, C.A., Hall, J.L., Geballe, T.R., 2000. Detection of daily clouds on Titan. Science 290, 509–513.

Griffith, C.A., and 13 colleagues, 2006. Evidence for a polar ethane cloud on Titan. Science 313, 1620–1622.

Hanel, R., and 14 colleagues, 1981. Infrared observations of the saturnian system from Voyager-1. Science 212, 192–200.

Hudson, P.K., Shilling, J.E., Tolbert, M.A., Toon, O.B., 2002. Uptake of nitric acid on ice at tropospheric temperatures: Implications for Cirrus clouds. J. Phys. Chem. A 106, 9874–9882.

Hunten, D.M., 2006. The sequestration of ethane on Titan in smog particles. Nature 443, 669–670.

Inaba, A., Koga, Y., Morrison, J.A., 1986. Multilayers of methane adsorbed on graphite. J. Chem. Soc. Faraday Trans. II 82, 1635–1646.

Iraci, L.T., Middlebrook, A.M., Tolbert, M.A., 1995. Laboratory studies of the formation of polar stratospheric clouds: Nitric acid condensation on thin sulfuric acid films. J. Geophys. Res. 100, 20969–20977.

Jain, P.C., Lee, S.K., Hozhabri, N., Sharma, S.C., 1994. Positron-annihilation study of phase transitions in ethane physisorbed on grafoil. Phys. Res. B 49, 2821–2824.

Khare, B.N., Sagan, C., Arakawa, E.T., Suits, F., Callcott, T.A., Williams, M.W., 1984. Optical-constants of organic tholins produced in a simulated titanian atmosphere—From soft-X-ray to microwave-frequencies. Icarus 60, 127–137.

Legagneaux, L.A., Cabanes, A., Domine, F., 2002. Measurement of the specific surface area of 176 snow samples using methane adsorption at 77 K. J. Geophys. Res. 107, 4335–4350.

Lorenz, R.D., and 39 colleagues, 2006. The sand seas of Titan: Cassini RADAR observations of longitudinal dunes. Science 312, 724–727.

Lysek, M.J., Lamadrid, M., Day, P., Goodstein, D., 1992. Adsorption hysteresis, capillary condensation, and melting in multilayer methane films on graphite foam. Langmuir 8, 898–900.

McKay, C.P., 1996. Elemental composition, solubility, and optical properties of Titan's organic haze. Planet. Space Sci. 44, 741–747.

Mitri, G., Showman, A.P., Lunine, J.I., Lorenz, R.D., 2007. Hydrocarbon lakes on Titan. Icarus 186, 385–394.

Moses, J.I., Allen, M., Yung, Y.L., 1992. Hydrocarbon nucleation and aerosol formation in Neptune atmosphere. Icarus 99, 318–346.

Niemann, H.B., and 17 colleagues, 2005. The abundances of constituents of Titan's atmosphere from the GCMS instrument on the Huygens probe. Nature 438, 779–784.

Pearl, J., Ngoh, M., Ospina, M., Khanna, R., 1991. Optical-constants of solid methane and ethane from 10,000 to 450 cm^{-1}. J. Geophys. Res. Planets 96, 17477–17482.

Porco, C.C., and 35 colleagues, 2005. Imaging of Titan from the Cassini spacecraft. Nature 434, 159–168.

Signorell, R., Jetzki, M., 2007. Phase behavior of methane haze. Phys. Rev. Lett. 98. 013401.

Stofan, E.R., and 37 colleagues, 2007. The lakes of Titan. Nature 445, 61–64.

Tokano, T., McKay, C.P., Neubauer, F.M., Atreya, S.K., Ferri, F., Fulchignoni, M., Niemann, H.B., 2006. Methane drizzle on Titan. Nature 442, 432–435.

Tomasko, M.G., and 39 colleagues, 2005. Rain, winds and haze during the Huygens probe's descent to Titan's surface. Nature 438, 765–778.

Toon, O.B., McKay, C.P., Courtin, R., Ackerman, T.P., 1988. Methane rain on Titan. Icarus 75, 255–284.

Trainer, M.G., Pavlov, A.A., DeWitt, H.L., Jimenez, J.L., McKay, C.P., Toon, O.B., Tolbert, M.A., 2006. Organic haze on Titan and the early Earth. Proc. Natl. Acad. Sci. 103, 18035–18042.

Waite, J.H., Young, D.T., Cravens, T.E., Coates, A.J., Crary, F.J., Magee, B., Westlake, J., 2007. The process of tholin formation in Titan's upper atmosphere. Science 316, 870–875.

West, R.A., Brown, M.E., Salinas, S.V., Bouchez, A.H., Roe, H.G., 2005. No oceans on Titan from the absence of a near-infrared specular reflection. Nature 436, 670–672.

Zondlo, M.A., Hudson, P.K., Prenni, A.J., Tolbert, M.A., 2000. Chemistry and microphysics of polar stratospheric clouds and cirrus clouds. Annu. Rev. Phys. Chem. 51, 473–499.